Study of Membrane Protein Monolayers Using Surface-Enhanced Infrared Absorption Spectroscopy (SEIRAS): Critical Dependence of Nanostructured Gold Surface Morphology

Ana Seiça, Muhammad Haseeb Iqbal, Alain Carvalho, Jun-Yong Choe, Fouzia Boulmedais, Petra Hellwig

Study of membrane proteins monolayers using surface-enhanced infrared absorption spectroscopy (SEIRAS): critical dependence of nanostructured gold surface morphology

Ana F. S. Seiça, *† Muhammad Haseeb Iqbal, ‡ Alain Carvalho, ‡ Jun Yong-Choe, ¶ Fouzia Boulmedais, ‡ Petra Hellwig *, †, ‖.

† Laboratory of Bioelectrochemistry and Spectroscopy, UMR 7140 University of Strasbourg CNRS, 4 Rue Blaise Pascal, 67081 Strasbourg, France.

‖ University of Strasbourg Institute for Advanced Studies (USIAS)

‡ University of Strasbourg, CNRS, Institut Charles Sadron, UPR 22, 67034 Strasbourg, France

¶ East Carolina Diabetes and Obesity Institute, East Carolina University, Greenville, NC 27834, USA

KEYWORDS: protein immobilization, self-assembled monolayer, enhancement factor, scanning electron microscopy, atomic force microscopy

ABSTRACT: Surface-enhanced infrared absorption spectroscopy (SEIRAS) is a powerful tool that allows studying the reactivity of protein monolayers at very low concentration and independent from the proteins size. In this study, we probe the surface's morphology of electroless gold deposition for optimum enhancement using two different types of immobilization adapted to two proteins. Independently from the mode of measurement (i.e., transmission or reflection) or type of protein immobilization (i.e, through electrostatic interactions or Nickel HisTag), the enhancement and reproducibility of the protein signals in the infrared spectra critically depended on the gold nanostructured surface morphology deposited on silicon. Just a few seconds deviation from the optimum time in the nanoparticle deposition led to a significantly weaker enhancement. Scanning electron microscopy and Atomic Force microscopy measurements revealed the evolution of the nanostructured surface when comparing different deposition times. The optimal deposition time lead to isolated gold nanostructures on the silicon crystal. Importantly in the case of the immobilization using Nickel HisTag, the surface morphology is rearranged upon immobilization of linker and the protein. A complex 3D network of nanoparticles decorated with the protein could be observed leading to the optimal enhancement. The electroless deposition of gold is a simple technique, which can be adapted to flow cells, and used in analytical approaches.

Fourier transform infrared (FTIR) spectroscopy provides vibrational information on an entire biomacromolecule under physiological conditions. The infrared (IR) irradiation is harmless to the sample, making it a powerful method for studying the structural changes of the biomacromolecules.[1] However, IR spectroscopy suffers from limited sensitivity in detecting the molecular structural changes at a monolayer level. Surface-enhanced infrared absorption spectroscopy (SEIRAS) was developed to detect structural changes of adsorbed or immobilized biomacromolecules.[2,3] The study of covalently immobilized protein monolayers on gold-coated silicon was established.[4-8] With SEIRAS, the adsorbed monolayer on a nanostructured metal film provided signal enhancement factors of 10 to 500,[9] allowing the detection of small spectral changes of the adsorbed protein.[10] The surface selection rules of SEIRAS imply that only the vibrations producing a dynamic dipole moment perpendicular to the surface will be enhanced, which allows, for example, to determine the binding and orientation of adsorbed molecules at the surface and the interface.[11] The enhancement of SEIRAS is restricted to a short distance from the surface (decay length of ± 8 nm),[12] eliminating the vibrational contributions from the bulk solution in the IR spectrum[5] and allowing to selectively detect signals from the adsorbed monolayer.[9, 11, 13-14]

The preparation of a thin metal film (< 5 nm) is the most critical part of a successful SEIRAS experiment since the absorption band of surface plasmons does not extend to the mid-IR region.[15, 16] The chemical enhancement putatively results from the charge transfer between the biomolecule and the Fermi level of the metals, which changes the charge distribution, and, thus, the dipole moment of the adsorbed molecules.[17, 18] Enhancement by SEIRAS depends on the size, shape, and particle density of the selected metal-island film.[19, 20] These properties are easily affected by the experimental conditions during film fabrication, including the rate of film deposition, the type of substrate, the substrate temperature, etc.[21] Controlling the deposition rate is essential for optimum enhancement. A slow deposition usually results in better enhancement.[21] Chemical (electroless) deposition leads to stable SEIRA-active thin films of Au and a stronger adhesion of the deposited metal layer to the substrate.[15, 21]

When using SEIRAS for the study of proteins, it is essential to chemically modify the bare metal since the interaction of the protein with the metal may induce denaturation. The so-called SAM (self-assembled monolayer) is an approach often used to tackle these obstacles.[22] The modified surface is produced by immersing the SEIRA-active metal substrate in a solution containing the crosslinker molecule. The SAM of the crosslinker is formed spontaneously by quasi-covalent bonding between the sulfur and the metal surface.[19] Direct covalent linking of the protein is also possible by attaching a nitrilotriacetic (NTA) moiety to the metal via a sulfhydryl group at the other end.[13] After complex formation with Ni^{2+}, a recombinant protein engineered with a polyhistidine tag at the C- or N-terminus can attach to the surface through the affinity of the tag for the Ni–NTA moiety. Polyhistidine tags are often used for protein purification,[23] and subsequent investigation of almost any soluble protein.[24, 25] Through the affinity of the genetically introduced

His-tag for the Ni^{2+}-NTA surface, the Ni-NTA immobilization procedure has the advantage of directing the orientation of the protein in the surface. The affinity of individual Ni-NTA to His-tags is usually low. However, when a support surface has a high density of immobilized Ni-NTA, multiple linkages by a His tagged protein provides a higher affinity and long-lasting association.[26] Using Ni^{2+}-NTA to immobilize membrane transport proteins allowed us to investigate protein protonation changes with the reaction-induced IR technique.[27, 28] This method has been applied to identify several critical residues in the proton path of membrane proteins,[29, 30] and water molecules. [31]

Despite all the successful SEIRAS studies, a major problem remains: the enhancement of the infrared absorption bands is not very reproducible, since even small variations in the experimental conditions during the formation of the rough metal surface lead to a significant decrease in the enhancement.[9, 32, 33] It has been shown that the Au and HF concentrations in the solutions used during the deposition process affect the deposition properties.[34] Temperature and deposition time have been shown to affect the gold morphology and orientation. For a better control of these phenomena a stronger understanding of the organization and the morphology of the SEIRAS active metal film is needed, together with the study of the interface between biomolecules and substrate, where the essential signal relay between the two different materials occurs. A potential influence of the protein deposition has not been studied yet, to best of our knowledge.

Here, we probe the surface's morphology of electroless gold deposition for optimum enhancement using two different types of immobilization adapted to proteins. The first protein was cytochrome *C* (Cyt *C*), a soluble protein that functions as an electron transfer protein in the so-called respiratory chain. For soluble proteins, SAMs of x-functionalized alkanethiols or disulfides represent the most versatile immobilization platform.[35] This well-characterized and highly stable protein can be easily immobilized via chemisorption on SAMs. [13, 36] Adsorbed Cyt *C* on a self-assembled monolayer (SAM) of 11-mercaptoundecanoic acid (11-MUA), bound on a gold surface, result in a SAM with high electronegativity which can affect the electron transfer property of adsorbed Cyt *C*.[37]

The second protein was a membrane transporter belonging to the Major Facilitator Superfamily (MFS), highly specific for glucose, the Staphylococcus epidermidis glucose/H^+ symporter ($GlcP_{Se}$).[38, 39] This predominately helical protein is a homolog of the human glucose transporters (SLC2 family).[40] The C-terminus of $GlcP_{Se}$ included a hexa-histidine tag (His-tag), useful to immobilize the protein directly on the modified gold surface. The membrane protein is solubilized in detergent, ensuring its structural integrity.

In this study, we compared the enhancement of IR signal obtained for adsorbed Cyt *C* on 11-MUA SAM and $GlcP_{Se}$ on Ni^{2+}-NTA SAM using attenuated total reflectance and transmittance mode. We show how a small variation of the deposition time (few seconds) of nanostructured gold change the SEIRAS enhancement in relation with important surface morphology changes. A surprisingly strong effect of the gold deposition time on the signal enhancement is reported independently from the mode of measurement or type of protein immobilization.

MATERIALS AND METHODS

Materials and Samples

Sodium tetrachloroaurate(III) dihydrate (NaAuCl4.2H2O, 99% Sigma), 3,3-dithiodipropionic acid di(N-hydroxysuccinimide ester) (DTSP, Sigma), Nα,Nα-bis(carboxymethyl)-L-lysine (ANTA Sigma 97%), Nickel (II) perchlorate hexahydrate (Ni(ClO4)2. 6H2O Sigma), 11-mercaptoundecanoic acid (11-MUA, Sigma 98%), were used as received without further purification. The ATR holder silicon crystal was provided from Harrick Scientific Products (Ossinging, NY, USA), with reference number 1006762 and the silicon wafers were purchased from Crystal GmbH (Berlin, Germany).

Electroless deposition of a gold surface

Before the protein immobilization, a thin gold layer was formed by chemical deposition on the surface of a silicon crystal as described previously.[2, 8, 13, 14, 27]

Initially, silicon crystals were polished with finer grade 0.3-μm alumina, followed by rinsing with distilled water, acetone, and water again. The crystal was immersed in a solution containing ammonium fluoride (NH_4F) (wt/vol) 40% for 1 min to remove the Si oxide layer and terminate it with hydrogen. Then, the surface was rinsed with water and dried again.

The crystal and the plating solution were heated together at 65°C for 10 min. The solution is a 1:1:1 mix (vol/vol/vol) of 15 mM $NaAuCl_4$ + 150 mM Na_2SO_3 + 50 mM $Na_2S_2O_3$ + 50mM NH_4Cl, and 2% HF (wt/vol: 1 ml). The silicon prism was covered with the plating solution for a range of times between 5 to 60 s, and deposition was stopped by washing the crystal surface with water, followed by drying the surface with a stream of argon.

Scanning Electron Microscopy (SEM)

The samples were observed using a FE-SEM Hitachi SU8010 at 1kV. The images were collected with the SE-in lens detector.

Atomic Force Microscopy (AFM)

Atomic Force Microscopy Multimode Nanoscope IV from Bruker (Palaiseau, France) was used to characterize the AuNP samples deposited on silicon wafers. The AuNP samples were prepared with depositions times of 20, 40, and 60s and dried. To probe the samples' topography, tapping mode in dry state was selected using etched silicon tips (RTESPA-300 from Bruker; having a spring constant "k" of around 40 Nm 1). The images were obtained preferably along the fast scan axis at a scan rate of 0.75 Hz with a resolution of 256x256 pixels. The data analysis was performed using NanoScope Analysis Software (version 1.7). The silicon wafers were previously cleaned by dipping in 50% (v/v) ethanol/water mixture for 15 min, followed by activation using a plasma cleaner for 3 min before their use.

Protein purification

$GlcP_{Se}$ wild type (WT) gene was cloned into the pET-15b vector (Novagen), expressed in E. coli C41 cells and purified as previously described (32). Purified $GlcP_{Se}$ at 12 mg/ml concentration was in 50mM KPi buffer at pH 7.0. Cytochrome *C* from bovine

heart was purchased from Sigma Aldrich and dissolved in 10 mM KPi with a final pH 8.0 and a concentration of 2 mM.

Immobilisation via Nickel-HisTag

After forming a gold layer on the silicon crystal, a nickel nitrilotriacetic acid self-assembled monolayer (Ni-NTA SAM) was deposited on the surface by adapting the procedure described in refs.[14, 27]

First, 1 mg/ml of 3,3-dithiodipropionic acid di(N-hydroxysuccinimide ester) (DTSP) in dimethyl sulfoxide (DMSO) was allowed to self-assemble on the gold surface. The monolayer formed after one hour. Excess DTSP was washed away with DMSO, and the crystal was dried under an argon stream. Afterward, the modified surface was immersed in a solution of 100 mM Nα,Nα-bis(carbox-ymethyl)-L-lysine (ANTA) in 0.5 M K_2CO_3 at pH 9.8 for 3 h and then rinsed with water. Finally, the surface was incubated in 50 mM Nickel (II) perchlorate hexahydrate ($Ni(ClO_4)_2$) solution for 1 h. After washing with water, the protein $GlcP_{Se}$ dissolved in 50 mM phosphate buffer, pH 7.5, containing 0.05% (w/v) n-dodecyl-beta-maltoside (DDM), was drop-casted on the modified surface.

Cyt C chemisorption.

After forming a gold layer, the silicon crystal was immersed in a solution containing 10 mM 11-mercaptoundecanoic acid (11-MUA). The monolayer was allowed to self-assemble for 2.5 h. Excess 11-MUA was re-moved and the crystal was rinsed with ethanol and gently dried with an argon stream. Finally, Cyt *C* was added to the modified surface, and the absorbance spectrum was recorded.

Infrared Spectroscopy

The two immobilization approaches were followed by FTIR in transmission or Attenuated Total Reflection (ATR) mode using different types of silicon crystals (Figure S1 in the SI). The silicon wafer with a 1 cm diameter (Figure S1.a) was used for the study of dry dried samples in transmission mode ~~(Figure S1.a in the SI).~~ After the deposition of the gold surface, the crystal was sealed in a metal support between two Teflon joints. Then, the cell was transferred to the spectrometer. The silicon crystal with 3-mm surface diameter (Figure S1.b) was used as a single reflection ATR unit, which allowed the simultaneous acquisition of FTIR spectra in the ATR mode and the perfusion of solutions with different compositions.[41]

All the experiments were carried out with a Bruker Vertex 70 FTIR spectrometer (Globar source, KBr beamsplitter, mercury cadmium telluride detector) with 8 mm aperture for ATR measurements and 6 mm for transmission and 40-kHz scanner velocity, 4 cm^{-1} resolution, and 256 scans.

Data treatment

In order to obtain the corresponding spectra of each mobilization step and the protein, the absorption spectra were used.
For the immobilization Nickel-Histag, the spectrum of DTSP linker was obtained as a reference spectrum the gold layer covered with DMSO, the second step was the lysine linker, where the spectrum was recorder with the DTSP SAM in water as a reference, the final linker, nickel, was recorded using the TSP-NTA SAM covered with water as a reference. The absorbance spectrum of the protein $GlcP_{Se}$ was recorded using the Ni-NTA modified gold layer as a reference
For the protein immobilized through chemisorption and followed both in transmission and ATR mode, the spectrum of an 11- MUA self-assembled monolayer was obtained suing as reference spectrum the gold layer. The absorbance spectrum of the protein Cyt C was recorded using the gold layer as a reference. For transmission experiments the spectra of the protein was recorded in dried, while for ATR mode, the spectra of the protein were recorded in buffer solution. For all the spectra shown, a baseline correction was performed, and the signals were smoothed for more clarity.
The enhancement factor was determined by using the amide I of each protein at different immobilizations as a factor. The EF was calculated using the area of the amide I band of the protein immobilized and the protein on the silicon crystal. This was done for both conditions (dry or in buffer solution) and for each different deposition time.

RESULTS

After the electroless deposition of gold on silicon and chemical modification with SAM, the IR spectra of adsorbed $GlcP_{Se}$ on Ni-NTA SAM and Cyt *C* on 11-MUA SAM were first recorded in dry state using transmittance mode and in liquid state using attenuated total reflectance (ATR) mode.

Surface-Enhanced IR Spectroscopy of adsorbed $GlcP_{Se}$ through Ni-NTA immobilization.

Figure 1.A1 shows the SEIRAS IR spectra obtained after each step of the $GlcP_{Se}$ immobilization procedure. After the self-assembly of DTSP, the signals in 1810, 1781, and 1736 cm^{-1} correspond to the succinimidyl group.[13] The addition of Nα,Nα-bis (carbox-ymethyl)-L-lysine (ANTA) lead to two new bands at 1615 and 1565 cm^{-1} (Figure 1.A2), corresponding to the amine's group reaction with the succinimidyl ester group of the DTSP to form an amide bond. The peak at 1390 cm^{-1} corresponds to the symmetric stretching mode of $\nu(COO^-)$ of ANTA carboxylate groups.[42, 43] As the final step before protein imobilization, Ni^{2+} complexation with the NTA surface led to small changes in the spectrum (Figure 1.A3) with the appearance of two bands at 1604 and 1402 cm^{-1} assigned to the asymmetric and symmetric stretching mode of the carboxylate groups of NTA that get deprotonated after complexation with Ni^{2+}.[13] These spectra correspond to the previously described immobilization process.[8, 14, 27] After immobilization of the $GlcP_{Se}$ protein, the characteristic amide I band appears[44] at 1650 cm^{-1} (Figure S2 in the SI). This signal includes coordinates from the C=O vibrational mode of the protein backbone. This protein-specific signal was used to study the dependence of the SEIRA enhancement factor with the gold deposition time (Figure 1.BC). To this aim, the Amide I band of $GlcP_{Se}$ protein on bare silicon crystal (without the metal film) was also registered in dry state in transmission mode and in solution in ATR mode (Figure S3A in the SI). In both cases, the 40s deposition time leads to the best enhancement.

The shape of the amide I band differs in both experiments (transmission/ reflection) mainly due to the different orientation that the protein can adopt relative to the surface. The inhomogeneous enhancement of the protein depends on the distance

from the surface. In general, anisotropic proteins can be adsorbed in different orientations. Elongated proteins may primarily be bound so that the long protein axis is oriented along or perpendicular to the surface. The former orientation is usually energetically favorable because the protein may form additional bonds to the surface.[45] Increased surface roughness may result in a higher proportion of proteins oriented perpendicular to the surface, leading to an increase of the saturation uptake because a protein needs less area to adsorb perpendicular to the surface. [46] Roughness and protein anisotropy can also enhance steric hindrance.[45]

Surface-Enhanced IR Spectroscopy of adsorbed Cyt *C* through 11-MUA immobilization

Another type of immobilization was used for the soluble protein Cytochrome *C*. A negatively charged 11-MUA SAM was created on nanostructured gold (Figure 2A.1). Presumably, the carboxylic groups of 11-MUA interact electrostatically with positively charged amino acids on the protein, for instance, lysine residues. Figure 2A.2 shows the corresponding SEIRA spectrum of the formation of the monolayer. The spectra display three peaks at 1701, 1463 and 1416 cm^{-1}, attributable to the ν(C=O) COOH and $\nu_s(COO^-)$, respectively. These positions suggest that protonated and deprotonated species are present on the surface.[47] Figure 2A.3 shows the absorbance spectrum of the protein Cyt *C* immobilized on an 11-MUA surface containing the characteristic bands, amide I and amide II, at 1640 and 1530 cm^{-1}, corresponding to the stretching vibration of the C=O groups and the stretching vibration of the C-N coupled to the NH in-plane bending, respectively.[44]

Figure 2BC shows the SEIRA spectra of the amide I band of Cyt *C* immobilized on 11-MUA SAM registered for the two IR modes at different gold deposition times. The results are comparable to those of $GlcP_{Se}$ immobilized on a Ni-NTA surface. In comparison to the adsorbed protein on bare silicon (Figure S3B), the best deposition time for the ideal protein signal enhancement is also 40s.

Analysis of the enhancement factor depending on the gold deposition time.

Figures 1BC and 2BC show the absorbance spectra of the amide I band of the two studied proteins, with observable shape, position, and intensity changes using two IR modes. To compare the results, we calculated the enhancement factor (EF) of the immobilized protein on the electroless deposited gold surface in comparison to bare silicon surface depending on the gold deposition time. Typically, the enhancement factor is often obtained by using a correction factor of the geometry of the surface to account for a different number of molecules bound to the probed sample area.[7, 48] The EF presented here corresponds to the lowest possible values and is typically higher if the exact geometrical arrangement of the gold surface is considered.[49] In transmission mode and dry state, the EF are between 0.6 and 1.6 for $GlcP_{Se}$ (Figure 1B) and 1.6 and 7 for Cyt C (Figure 2B) in comparison to bare silicon crystal. In ATR mode and liquid state, they are between 2.5 and 4.0 for $GlcP_{Se}$ (Figure 1C) and 1.1 and 1.5 for Cyt C (Figure 2C). For both IR modes, a maximum enhancement is obtained with a gold deposition time of 40 s. Obviously, a small variation of the reaction conditions strongly affects the enhancement factor. To elucidate this phenomenon, the electroless deposited gold surface was then characterized.

Morphological Characterization

The deposited gold on the silicon crystals were examined in depth by SEM and AFM (Figure 3), focusing on the coverage, dispersion, and the impact of the attachment layers. It is noted that the protocol used for the AFM and the SEM measurements corresponds to the one used to obtain the IR data of $GlcP_{Se}$ protein (Figure 1). SEM images show the formation of gold nanoparticles (AuNPs) on the surface of the silicon crystal for gold deposition time of 20, 40 and 60s (Figure 4A-C). The increase in the deposition time led to different morphologies of AuNPs. The observed nanoparticle density is low for short deposition time (20s). At longer deposition times (60s), the density increases and eventually saturates.

AFM revealed the round shape and isolated AuNPs of 54 ± 5 nm in diameter after 20s of gold deposition (Figure 3D). A higher density in AuNPs was obtained when the deposition time was increased to 40 s, leading to close contact of several nanoparticles (Figure 3E) as observed in SEM. At 60s of deposition, the silicon crystal was fully covered by a layer of gold underneath the isolated AuNPs forming agglomeration or a multilayer of gold nanostructures (Figure 3F and S4 in the SI). Whatever the deposition time, the size of the isolated nanoparticles is around 50 to 60 nm in diameter (horizontal distance) and with a height of around 20 nm (vertical distance) (Table S1). Increasing the deposition time from 20 to 40s led to the expected higher density of particles on the surface with a de-crease of the distance between the particles. We may suggest that the shorter distance between the particles is responsible for the higher enhancement of the protein signal observed with IR. At 60s of deposition, the underneath layer of gold probably prevented the enhancement of AuNPs.

Figure 4 shows the AFM images obtained after immobilization of $GlcP_{Se}$ protein through Ni^{2+}-NTA on AuNPs obtained after 40 s of deposition. Interestingly, the distance between the particles decreased and the nanostructures seem much larger after the Ni^{2+}-NTA immobilization (Figure 4A) in comparison to bare AuNPs (Figure 3E). The size of the nanoparticles increases from 49 ± 9 nm to 67 ± 5 nm in diameter (horizontal distance) with no increase in height (vertical distance) (Table S2). In the following, the topography of the surface changed drastically due to the adsorption of the proteins. In contrast to bare silicon surface (Figure S6 in the SI), the immobilization of $GlcP_{Se}$ protein on AuNPs-Ni^{+2}-NTA surface lead to both small and large aggregates covering entirely the nano-particles (Figure 4B). The larger aggregates are 202 ± 14 nm in diameter and 90 ± 6 nm in height. The AFM Peak Force error images, related to the phase differences, of the AuNPs surface before and after protein immobilization show a great difference (Figure S7). These images could give a qualitative evaluation of the hardness of the surface. AuNPs surface has small isolated bright areas with high rigidity. After $GlcP_{Se}$ protein immobilization through Ni^{+2}-NTA ligand, the AFM image showed a homogeneous surface with no bright areas. This confirms that all the AuNPs and the surface of the sample were totally covered by the protein. The enhancement of the IR signal observed in Figure 1 could be attributed

to these structures due to Ni^{+2}-NTA immobilization localizing the proteins on the surface of the nanoparticles.

DISCUSSION AND CONCLUSION

We report the SEIRAS of two differently immobilized proteins along with the analysis of the structure morphology with the optimum enhancement of the amide I signal. A low but reproducible enhancement of 1.5 to 7 was obtained for the amide I signal. Despite the modest enhancement factor, the surface obtained is typically of high stability allowing the use of difference spectroscopic approaches and studies of protein reactivity.[19]

In the experimental setup and the reaction conditions used (both transmission and ATR modes) an optimal deposition time of 40s for gold was found. SEM and AFM studies revealed how the surface changed when the deposition time was just a few seconds higher or lower. At 40s the crystal had sufficient surface coverage with the nanostructures and, hence, a high density of biofunctional molecules immobilized onto the surface. With longer deposition times, the inner surface area decreased due to the increasing connection between islands, resulting in reduced enhancement. According to,[50] the coefficient of the electric field enhancement is a function of the dielectric permeability of the metal. Simultaneously, the influence of the metal under some conditions and characteristics of the surface or adsorbed substances can lead not only to enhancement but also reduction in the optical transitions of the molecules near the metal surface.[24]

Previous studies focused on the characterization of deposited nanoparticles. Here we show that the immobilization process itself strongly modifies the surface features. Since the enhancement mechanism is based on the electric field rise near curved metal surface[51] the modification of the 3D structure is critical. A reorganization on the surface takes place and the size of the nanostructures changed after adding the protein. The interaction between proteins and nanoparticles is determined by the surface heterogeneity of the NPs, but also depends on the protein heterogeneity as well as its size.[52] Once the protein is adsorbed onto the surface of the AuNPs, they can alter the size, aggregation state, and interfacial properties of the nanomaterial.[53] It is noted that structures with a highly defined shape, including nanoarrays and nanoantenna's lead to a significantly higher enhancement,[54-56] however the creation of these surfaces is much more laborious.

The observations made in this study are important for a better understanding of the surface structure that induces ideal SEIRAS conditions. The obtained results demonstrate how easy is to prepare the gold nanostructures for a good enhancement of the protein signal which then can be adapted to flow cells and be used in analytical approaches. All of this is relevant in IR chem/bio sensing schemes. These findings will help enhancing the sensitivity of IR assay technologies by deliberately controlling SEIRA-based signal amplification. This has particular importance, if biomarkers of extremely low concentrations must be detected, like in neurodegenerative diseases such as Parkinson or Alzheimer disease. The potential of using a label-free mid-infrared protein conformation assay technology with enhanced sensitivity and chem/bio sensing is clear in this work.

Supporting Information

The Supporting Information is available free of charge

Different silicon crystal used for the immobilization of proteins; spectrum of the protein $GlcP_{Se}$ immobilized on the Ni-NTA surface and spectra of the proteins $GlcP_{Se}$ and Cytochrome C on the bare metal of silicon in dry state measured using ATR; Scanning electron microscopy image of a gold layer on a silicon of the electroless deposition of the gold on a silicon wafer after the immobilization of Ni^{2+}-NTA; AFM height images of electroless deposited AuNPs on a silicon crystal at 60 s deposition time. Characteristic size of electroless deposition of AuNPs on a silicon crystal at different deposition times; Characteristic size of electroless deposition of AuNPs on a silicon crystal for 40 s after Ni^{2+}-NTA and $GlcP_{Se}$ protein immobilization.

AUTHOR INFORMATION

Corresponding Author

* hellwig@unistra.fr +33 368 851273, UMR 7140, CMC, University of Strasbourg CNRS, 4 Rue Blaise Pascal 67081, Strasbourg, France.

Author Contributions

Ana Filipa Santos Seica performed experiments and contributed to the paper writing, Muhammad Haseeb Iqbal, performed AFM analysis, Alain Carvalho, performed SEM analysis, Jun-Yong, prepared samples, Fouzia Boulmedais, contributed to paper writing, Petra Hellwig, contributed to paper writing, and raised funding.

Funding Sources

AFSC and PH are grateful to the IDEX International doctoral program (PDI) from the University of Strasbourg, USIAS, the FRC ANR-10- 438 LABX-0026-CSC). M.H.I. thanks the Higher Education Commission's (HEC) Pakistan for his Ph.D.

ABBREVIATIONS

SEIRAS, Surface-enhanced infrared absorption spectroscopy; SAM, self-assembled monolayer; EF, enhancement factor; SEM, scanning electron microscopy; AFM, atomic force microscopy; FTIR, Fourier transform infrared spectroscopy; IR, infrared spectroscopy; NTA, nitrilotriacetic; MUA, 11-mercaptoundecanoic acid; MFS, Major Facilitator Superfamily; $GlcP_{Se}$, *Staphylococcus epidermidis* glucose/H^+ symporter; ATR, Attenuated Total Reflection;

REFERENCES

(1) Siebert, F.; Hildebrandt, P. Vibrational Spectroscopy in Life Science. **2008**, Weinheim: Wiley-VCH, 4-10.

(2) Ataka, K.; Stripp, T. S.; Heberle, J. Surface-enhanced infrared absorption spectroscopy (SEIRAS) to probe monolayers of membrane proteins, *Biochimica et Biophysica Acta (BBA) – Biomembranes*. **2013**, 1828(10), 2283-2293.

(3) Lorenz-Fonfria, V. A. Infrared Difference Spectroscopy of Proteins: From Bands to Bonds. *Chem. Rev*. **2020,** 120(7), 3466-3576.

(4) Ataka, K.; Heberle, J. Use of Surface Enhanced Infrared Ab-sorption Spectroscopy (SEIRA) to probe the functionality of a protein monolayer. *Biopolymers.* **2006,** 82, 415-419.

(5) Brown, C. W.; Li, Y.; Seelenbinder, J. A.; Pivarnik, P.; Rand, A. G.; Letcher, S. V.; Gregory, O. J.; Platek, M. J. Immunoassays Based on Surface-Enhanced Infrared Absorption Spectroscopy. *Anal. Chem.* **1998,** 70, 2991-2996.

(6) Kuhne, C.; Steiner, G.; Fischer, W. B.; Salzer, R. Surface enhanced FTIR spectroscopy on membranes. *Fresenius' J. Anal. Chem.* **1998,** 360, 750–754.
(7) Dovbeshko, G. I.; Chegel, V. I.; Gridina, N. Y.; Repnytska, O. P.; Shirshov, Y. M.; Tryndiak, V. P. Surface Enhanced IR Absorption of Nucleic Acids From Tumor Cells: FTIR Reflectance Study. *Biopolymers*. **2002**, 67(6), 470-86.
(8) Seica, A. F. S.; Schimpf, J.; Friedrich, T.; Hellwig, P. Visualizing the movement of the amphipathic helix in the respiratory complex I using a nitrile infrared probe and SEIRAS. *FEBS Lett.* **2020**, 594(3), 491-496.
(9) Osawa, M.; Ataka, K. Electromagnetic Mechanism of Enhanced Infrared-Absorption of Molecules Adsorbed on Metal Island Films. *Surf. Sci.* **1992**, 262, L118−L122.
(10) Ataka, K.; Kottke, T.; Heberle, J. Thinner, Smaller, Faster: IR Techniques To Probe the Functionality of Biological and Biomimetic Systems. *Angew. Chem. Int. Ed*. **2010**, 49(32): 5416–5424.
(11) Osawa, M.; Ataka, K. I.; Yoshii, K.; Nishikawa, Y. Surface-Enhanced Infrared Spectroscopy: The Origin of the Absorption Enhancement and Band Selection Rule in the Infrared Spectra of Molecules Adsorbed on Fine Metal Particles. *Appl. Spectrosc*. **1993**, 47, 1497-1502.
(12) Osawa, M. In Handbook of Vibrational Spectroscopy; Chalmers, J. M.; Griffiths, P. R., Eds.; Wiley: Chichester. **2002**, Vol. 1, pp. 785-799.
(13) Ataka, K.; Giess, F.; Knoll, W.; Naumann, R.; Haber-Pohlmeier, S.; Richter, B.; Heberle, J. Oriented Attachment and Membrane Reconstitution of His-tagged Cytochrome C Oxidase to a Gold Electrode: In Situ Monitoring by Surface-Enhanced Infrared Absorption Spectroscopy. J. *Am. Chem. Soc.* **2004**, 126(49), 16199-206.
(14) Kriegel, S.; Uchida, T.; Osawa, M.; Friedrich, T.; Hellwig, P. Biomimetic Environment to Study E. Coli Complex I Through Surface-Enhanced IR Absorption Spectroscopy. *Biochem*. **2014**, 53(40), 6340-7.
(15) Osawa, M.; Ikeda, M. Surface-enhanced infrared absorption of p-nitrobenzoic acid deposited on silver island films: contributions of electromagnetic and chemical mechanisms. *J. Phys. Chem.* **1991**, 95(24), 9914–9919.
(16) Osawa, M. Dynamic Processes in Electrochemical Reactions Studied by Surface-Enhanced Infrared Absorption Spectroscopy (SEIRAS). *Bull. Chem. Soc. Jpn*. **1997**, 70, 2861–2880.
(17) Skibbe, O.; Binder, M.; Otto, A.; Pucci, A. Electronic contributions to infrared spectra of adsorbate molecules on metal surfaces: Ethene on Cu(1 1 1). *J. Chem. Phys.* **2008,** 128, 194703, DOI: 10.1063/1.2912186.
(18) Merklin, G. T.; Griffiths, P. R. Influence of Chemical Interactions on the Surface-Enhanced Infrared Absorption Spectrometry of Nitrophenols on Copper and Silver Films. *Langmuir*. **1997,** 13, 6159–6163.
(19) Ataka, K.; Heberle, J. Biochemical applications of surface-enhanced infrared absorption spectroscopy. *Anal Bioanal Chem*. **2007**, 388(1), 47-54.
(20) Miyake, H.; Ye, S.; Osawa, M. Electroless deposition of gold thin films on silicon for surface-enhanced infrared spectroelectrochemistry. *Electrochem. Commun.* **2002**, 4(12), 973-977.
(21) Nishikawa, Y.; Nagasawa, T.; Fujiwara, K.; & Osawa, M. Silver island films for surface-enhanced infrared absorption spectroscopy: effect of island morphology on the absorption enhancement. *Vib. Spectrosc.* **1993,** 6(1), 43-53.
(22) Pinkerneil, P.; Guldenhaupt, J.; Gerwert, K.; Kotting, C. Surface-Attached Polyhistidine-Tag Proteins Characterized by FTIR Difference Spectroscopy. *Chem. Phys. Chem***. 2012**, 13, 2649-2653.
(23) Bornhorst, J. A.; Falke, J. J. Applications of Chimeric Genes and Hybrid Proteins, Part A Methods in Enzymology. **2000**, Vol. 326, Elsevier, Amsterdam, p. 245.
(24) Bondar, V. V.; Kuryk, M. V. Exciton luminescence on the interface antracene-gold. *J. Exp. Theor. Phys*. **1980**, 78(1), 94–99.
(25) Ataka, K.; Richter, B.; Heberle, J. Orientational Control of the Physiological Reaction of Cytochrome c Oxidase Tethered to a Gold Electrode. *J. Phys. Chem. B*. **2006**, 110(18), 9339-9347.
(26) Bornhorst, J. A.; Falke, J. J. Purification of proteins using polyhistidine affinity tags. *Methods in enzymology*. **2000**, 326, 245-254.
(27) Grytsyk, N.; Seiça, A. F. S.; Sugihara, J.; Kaback, H. R.; Hellwig, P. Arg302 governs the pKa of Glu325 in LacY. *P.N.A.S.* **2019**, 116(11), 4934-4939.
(28) Seica, A. F. S.; Iancu, C. V.; Pfeilschifter, B.; Madej, M. G.; Choe, J. Y.; Hellwig, P. Asp22 drives the protonation state of the Staphylococcus epidermidis glucose/H^+ symporter. *J Biol Chem*. **2020,** 295(45): 15253-15261.
(29) Iwaki, M.; Giotta, L.; Akinsiku, A. O.; Schägger, H.; Fisher, N.; Breton, J.; Rich, P. R. Redox-induced transitions in bovine cytochrome bc1 complex studied by perfusion-induced ATR-FTIR spectroscopy. *Biochem***. 2003**, 42(38): 11109–11119.
(30) Siebert, F.; Mäntele, W.; Gerwert, K. Fourier-transform infra-red spectroscopy applied to rhodopsin. The problem of the protonation state of the retinylidene Schiff base re-investigated. *Eur. J. Biochem*. **1983**, 136(1): 119-127.
(31) Wolf, S. F. E.; Cui, Q.; Gerwert, K. Infrared spectral marker bands characterizing a transient water wire inside a hydrophobic membrane protein. *J. Chem. Phys*. **2014**, 141(22): 22D524, DOI: 10.1063/1.4902237.
(32) Enders, D.; Pucci, A. Surface Enhanced Infrared Absorption of Octadecanethiol on Wet-Chemically Prepared Au Nanoparticle Films. *Appl. Phys. Lett*. **2006**, 88, 184104, DOI: 10.1063/1.2201880
(33) Gauglitz, G. Critical assessment of relevant methods in the field of biosensors with direct optical detection based on fibers and waveguides using plasmonic, resonance, and interference effects. *Anal Bioanal Chem.* **2020**, 412, 3317–3349.
(34) Lahiri, A.; Kobayashi, S.-I. Electroless deposition of gold on silicon and its potential applications: review. *Surf. Eng.* **2016**, 32(5): 321-337.
(35) Mohamad, N. R.; Marzuki, N. H. C.; Buang, N. A.; Huyop, F.; Wahab, R. A. An overview of technologies for immobilization of enzymes and surface analysis techniques for immobilized enzymes. *Biotechnol Biotechnol.* **2015**, 29(2), 205-220.
(36) Nakano, K.; Yoshitake, T.; Yamashita, Y.; & Bowden, E. F. Cytochrome c Self-Assembly on Alkanethiol Monolayer Electrodes as Characterized by AFM, IR, QCM, and Direct Electrochemistry. *Langmuir.* **2007**, 23(11), 6270-6275.
(37) Jiang, X.; Ataka, K.; Heberle, J. Influence of the Molecular Structure of Carboxyl-Terminated Self-Assembled Monolayer on the Electron Transfer of Cytochrome c Adsorbed on an Au Electrode: In Situ Observation by Surface-Enhanced Infrared Absorption Spectroscopy. J. *Phys. Chem. C*. **2008**, 112(3), 813-819.
(38) Lodish, H.; Berk, A.; Zipursky, S. L.; Matsudaira, P.; Baltimore, D.; Darnell J. Overview of Membrane Transport Proteins. Molecular Cell Biology**. 2000**, 4th edition. New York: National Center for Biotechnology Information, Bookshelf.
(39) Iancu, C. V.; Zamoon, J.; Woo, S. B.; Aleshin, A.; Choe, J. Y. Crystal structure of a glucose/H+ symporter and its mechanism of action. *P.N.A.S.* **2013**, 110(44), 17862-17867.
(40) Mueckler, M.; Thorens, B. The SLC2 (GLUT) family of membrane transporters. *Mol. Aspects Med*. **2013**, 34(2-3), 121-38.
(41) Furutani, Y.; Kimura, T.; Okamoto, K. Development of a rapid Buffer-exchange system for time-resolved ATR-FTIR spectroscopy with the step-scan mode. *Biophysics (Nagoyashi).* **2013**, 9, 123-129.
(42) Venyaminov, S.Y.; Kalnin, N. N. Quantitative IR spectrophotometry of peptide compounds in water (H2O) solutions. II. Amide absorption bands of polypeptides and fibrous proteins in alpha-, beta-, and random coil conformations. *Biopolymers.* **1990**, (13-14), 1259-1271.
(43) Wolpert, M.; Hellwig, P. Infrared spectra and molar absorption coefficients of the 20 alpha amino acids in aqueous solutions in the spectral range from 1800 to 500 cm^{-1}. *Spectrochimica Acta Part A: Molecular and Biomolecular Spectroscopy*. **2006**, 64(4): 987-1001.
(44) Fabian, H., Mäntele, W. **(2006).** Infrared spectroscopy of proteins. Handbook of vibrational spectroscopy, DOI: 10.1002/0470027320.s8201

(45) Rechendorff, K.; Hovgaard, M. B.; Foss, M.; Zhdanov, V. P.; Besenbacher, F. Enhancement of Protein Adsorption Induced by Surface Roughness. *Langmuir*. **2006**, 22(26), 10885-10888.
(46) Scopelliti, P. E.; Borgonovo, A.; Indrieri, M.; Giorgetti, L.; Bongiorno, G.; Carbone, R.; Podestà, A.; Milani, P. The effect of surface nanometre-scale morphology on protein adsorption. *PloS one*. **2010**, 5(7), e11862, DOI: 10.1371/journal.pone.0011862
(47) Stettner, J.; Frank, P.; Griesser, T.; Trimmel, G.; Schennach, R.; Gilli, E.; Winkler, A. A Study on the Formation and Thermal Stability of 11-MUA SAMs on Au(111)/Mica and on Polycrystalline Gold Foils. *Langmuir*. **2009**, 3, 1427-1433.
(48) Dovbeshko, G. I.; Paschuk, O. P.; Fesenko, O. M.; Chegel, V. I.; Shirshov, Y. M.; Nazarova, A. A.; Kosenkov, D. V. Biological Molecule Conformations Probed and Enhanced by Metal and Carbon Nanostructures: SEIRA, AFM and SPR Data. In: Buzaneva E., Scharff P. (eds) Frontiers of Multifunctional Integrated Nanosystems. NATO Science Series II: Mathematics, Physics and Chemistry. **2004**, vol 152. Springer, Dordrecht, 447-466.
(49) Dovbeshko, G.; Shirshov, Y. M.; Chegel, V.; Fesenko, O. Experimental and calculated enhancement factor in the SEIRA method. Proc. SPIE 5507, XVI International Conference on Spectroscopy of Molecules and Crystals, **2004**, DOI: 10.1117/12.570019
(50) Kosobukin, V. A. Effect of enhancement of external electric field near metal surface and its manifestation in spectroscopy. *Surface. Physics, chemistry, mechanics*. **1983**, 12, 5-20.
(51) Dovbeshko, G. I.; Fesenko, O. M.; Shirshov, Y. M.; Chegel, V. I. The enhancement of optical processes near rough surface of metals. *Semiconductor Physics, Quantum Electronics & Optoelectronics*. **2004**, 7(4), 411-424.
(52 Huang, R.; Carney, R. P.; Stellacci, F., Lau, B. L. T. Protein-nanoparticle interactions: the effects of surface compositional and structural heterogeneity are scale dependent. *Nanoscale*. **2013**, 5: 6928–6935.
(53) Doctor, D.; Westmeier, D.; Markiewicz, M.; Stolte, S.; Knauer, S. K.; Stauber, R. H. The nanoparticle biomolecule corona: Les-sons learned—challenge accepted? *Chem. Soc. Rev*. **2015**, 44: 6094–6121.
(54) Omeis, F., Seica, A. F. S.; Bernard, R., Javahiraly, N.; Majjad, H.; Moss, D.; Hellwig, P. Following the Chemical Immobilization of Membrane Proteins on Plasmonic Nanoantennas Using Infrared Spectroscopy. *ACS Sens*. **2020**, 5(7): 2191-2197.
55) Neubrech, F.; Huck, C.; Weber, K.; Pucci, A.; Giessen, H. Surface-Enhanced Infrared Spectroscopy Using Resonant Nanoantennas. *Chem Rev*. **2017**, 117(7): 5110-5145.
56) Adato, R.; Yanik, A. A.; Amsden, J. J.; Kaplan, D. L.; Omenetto, F. G.; Hong, M. K.; Erramilli, S.; Altug, H. Ultra-sensitive vibrational spectroscopy of protein monolayers with plasmonic nanoantenna arrays. *P.N.A.S.* **2009**, 106(46): 19227-32.

Figures

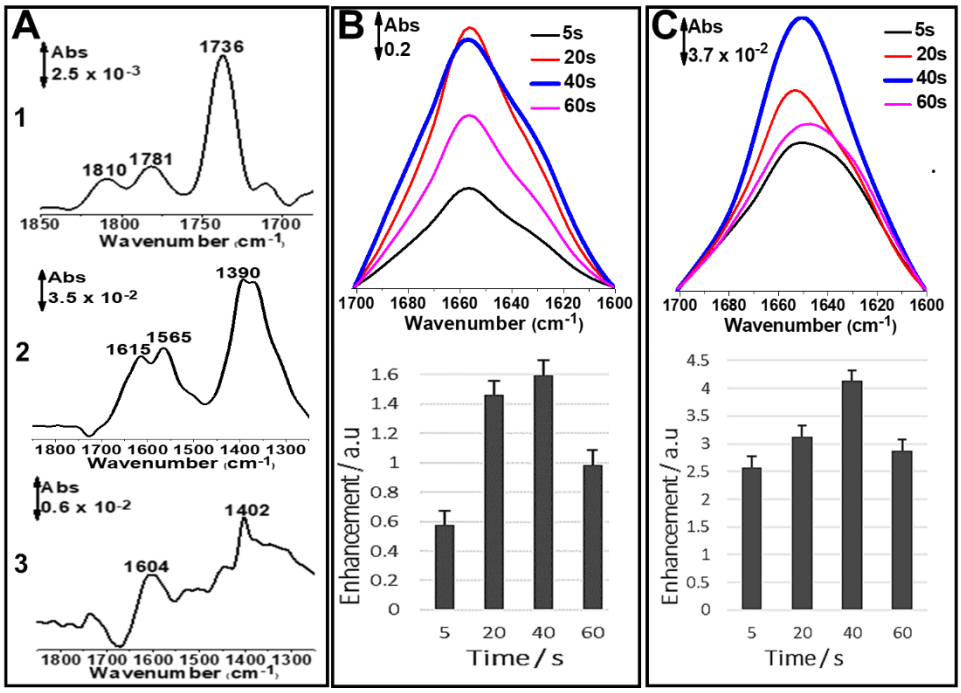

Figure 1: Spectra of the surface modification process followed by attenuated total reflection. (A) Self-assembly of the TSP monolayer on the bare Au surface (1), Cross-linking of ANTA with the TSP monolayer (2), complexation of Ni^{2+} by NTA (3). Absorbance spectra of Amide I band of the protein $GlcP_{Se}$ immobilized on a Ni-NTA surface as a function of the gold deposition time on different crystals. (B) Spectra of the protein dried measured in transmission (C) Spectra of the protein measured in ATR mode. Enhancement factor of the protein in transmission and ATR mode at different time deposition of the gold.

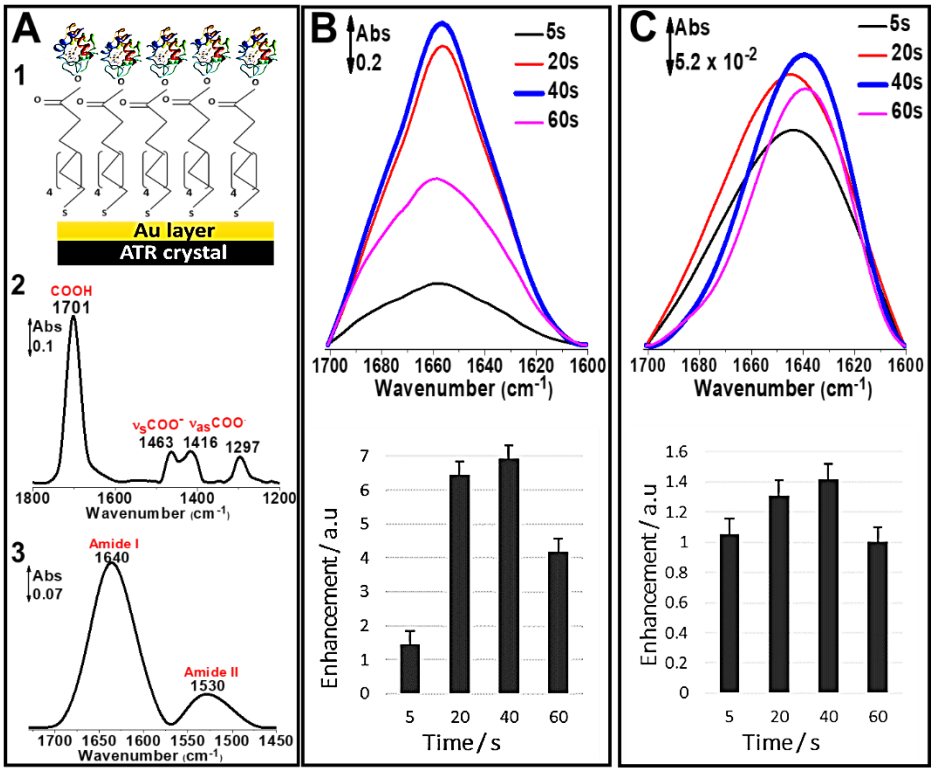

Figure 2: A.1) Schematic image of the protein Cytochrome C immobilized on an 11-MUA self-assembled monolayer gold surface. A.2) Spectrum of an 11-mercaptoundecanoic acid (MUA) self-assembled monolayer on a gold surface. A.3) Absorbance spectrum of the protein Cyt C immobilized on an 11-MUA surface. B and C) Absorbance spectra of Amide I band of Cytochrome *C* protein immobilized on a 11-MUA surface in transmission (B) and in ATR mode (C)) as a function of the gold deposition time on different crystals. Enhancement factor of the protein in transmission and ATR mode at different time deposition of the gold.

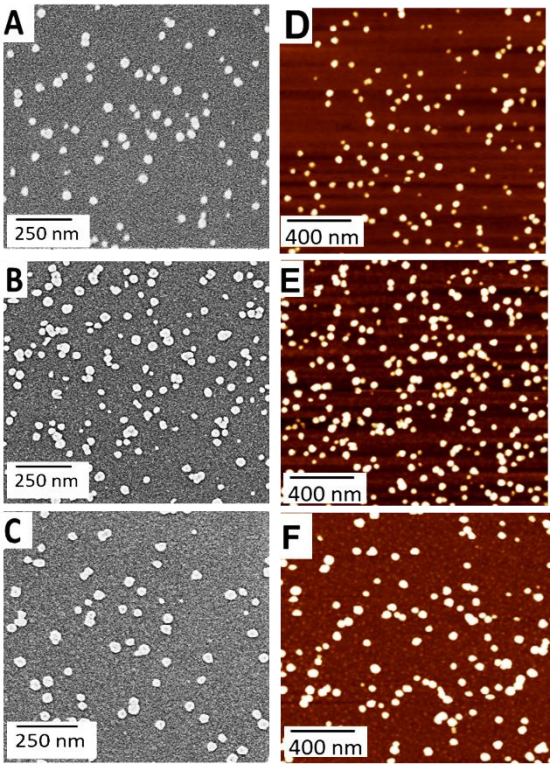

Figure 3: Electroless deposition of gold nanoparticles on a silicon crystal at different deposition times, 20 (A, D), 40 (B, E) and 60sec (C, F). Scanning electron microscopy image of a gold layer on a silicon of the electroless deposition of the gold on a silicon wafer before the immobilization of Ni^{2+}-NTA (left). AFM 2D images obtained in tapping mode and dry state with z scale of 30 nm of the electroless deposition of the gold on a silicon wafer before the immobilization step (right).

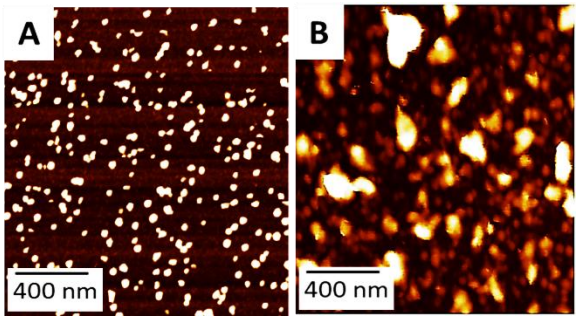

Figure 4: AFM 2D images obtained in tapping mode and liquid state of the electroless deposition of the gold on a silicon wafer at 40 s after immobilization (A) of Ni^{2+}-NTA with z scale of 30 nm followed by (B) the protein $GlcP_{Se}$ with z scale of 70 nm.